Marine Geophysical Research (2024) 45:15
https://doi.org/10.1007/s11001-024-09549-0

ORIGINAL RESEARCH PAPER

Seismo-stratigraphic and morpho-bathymetric analysis revealing recent fluid-rising phenomena on the Adventure Plateau (northwestern Sicily Channel)

Mariagiada Maiorana[1] · Daniele Spatola[2] · Simona Todaro[1] · Francesco Caldareri[1] · Fabrizio Parente[1] · Alessandro Severini[3] · Attilio Sulli[1]

Received: 16 November 2023 / Accepted: 31 May 2024

Abstract

The northwestern region of the Sicily Channel hosts a great number of morphological highs, the widest of which is the Adventure Plateau that is part of the Sicilian Maghrebian Fold and Thrust Belt system, formed since the Neogene. The Adventure Plateau was shaped in the Early Pliocene by an extensional phase that produced high-angle normal faults mostly WNW-ESE to N-S oriented. Through these faults, magmatic fluids ascended and produced widespread volcanic manifestations often associated to fluid flow processes. The interpretation of multibeam echosounder, seismic reflection (sparker, airgun) and well-log data allow us to identify several features related to the presence of fluids in the study area. The morpho-structural analysis showed a NW–SE oriented fault system and a string of pockmarks that follow the same trend. A detailed well-log analysis confirmed the presence of oil traces, at a depth of ~ 250 m, and gas (i.e., CO_2) at a depth of ~ 450 m. The seismo-stratigraphic analysis highlighted seismic signals located below the pockmarks, (e.g. seismic chimneys, bright spots) which suggest the presence of fluids that would rise to a few meters' depth. Based on the observations, two sources and two corresponding rising mechanisms have been identified. Morphometric analysis of pockmarks has been performed to delineate their possible interaction with the bottom currents. A fluids pathway model has been reconstructed, revealing the source of fluids emissions at depth in the Adventure Plateau, and providing new insights into the identification of fluid leakage pathways.

Keywords Pockmark · Seismic reflection profiles · Seismic chimney · Fluid seepage · Morpho-bathymetry

Introduction

Fluid flow and escape processes at the seafloor are widely and globally investigated phenomena affecting different geodynamic contexts (e.g., active and rifted continental margins, compression zones -subductions-, highly sedimented areas -deltas-), giving rise to diverse types of seabed morphologies, such as positive (e.g., mud volcanoes) or negative (e.g., pockmarks) features (Hovland 2011; Judd and Hovland 2007) as well as to a range of associated geological, geochemical and biological processes (Bünz et al. 2012; Hovland 2011; Judd and Hovland 2007; Sun et al. 2020).

Submarine fluid emissions occurring at the seafloor can be cold seeps, if refer to low-temperature emissions, lower than a few tens of degrees Celsius, and hot hydrothermal fluids, if reach 200 up to 400 °C. The main emitted gas is methane (CH_4) and secondarily carbon dioxide (CO_2) or nitrogen (N_2), either in the form of gas bubbles or dissolved gas (Claypool and Kaplan 1974; Judd and Hovland 2007). The methane generally originates from bacterial degradation of organic matter at low temperatures (biogenic gas) (Whiticar 1999, 2002), or thermogenic fluids produced from organic precursors at high temperature and pressure (Davis 1992; Etiope and Milkov 2004), CO_2 and N_2 are often related to hydrocarbon systems developed in proximity of subducting

✉ Mariagiada Maiorana
mariagiada.maiorana@unipa.it

1 Department of Earth and Marine Sciences, University of Palermo, Via Archirafi 22, 90123 Palermo, Italy

2 Department of Earth Sciences, Sapienza University, Piazzale Aldo Moro 5, 00185 Rome, Italy

3 7Seas Med Srl, Via Plinio 127, 74121 Taranto, Italy

Published online: 24 June 2024

slabs or final phases of thermogenic gas generation (Motyka et al. 1989).

The more recent geophysical tools in oceanic exploration such as multibeam echosounders, 2D and 3D high-resolution reflection seismics, imagine the water column, the seafloor (with information also on backscatter) and the sub-seafloor; these data allowed the mapping of fluid flow morphologies on continental margins and to reconstruct the migration patterns of the fluids to the seafloor. The seafloor depressions related to fluid flow detected from shallow to deep water via geophysical methods, direct observations (e.g., ROV images), and sediment and/or water samplings, are defined as pockmarks (Gentz et al. 2014; Judd and Hovland 2007; Spatola et al. 2017). They are strongly different in diameters and depths respectively from 150 m up to a few km (Sun et al. 2011), and have circular to elongate planform shapes, steep flanks, and flat to cone-shaped bottoms (Ceramicola et al. 2018; Ho et al. 2012; Micallef et al. 2022). The shape of pockmarks can be modified by the erosive action of the bottom currents (Miramontes et al. 2016; Picard et al. 2018). Pockmarks can be grouped in classes based on their size as follows (more deatil in Hovland et al. 2002):

(i) 'Unit-Pockmarks' to indicate very small depressions (1–10 m wide, and up to 0.6 m deep), usually isolated or organized in groups;
(ii) 'Normal pockmarks' generally bigger (10–700 m wide, and up to 45 m deep).
(iii) 'Giant Pockmarks' for depressions bigger than 250 m in diameter.

All the above-mentioned kinds of pockmarks can be found arranged in strings of pockmarks (up to a few km long). They often follow the weakness zones near-vertical faults, fractures or flexures (Hovland et al. 2002).

In the last years, evidence of fluid emissions has been recognized in the Sicily Channel around the Pantelleria Island, on the Graham Bank and on the Malta Plateau (Micallef et al. 2011; Savini et al. 2009; Conte et al. 2014; Spatola et al. 2018a, 2018b, 2023; Volpi et al. 2022; Ferrante et al. 2022; Civile et al. 2023), but the fluid flow process in the area is still poor known especially the mechanisms of migration of the fluids from deep sources to the seafloor and the role of the faults and/or fractures.

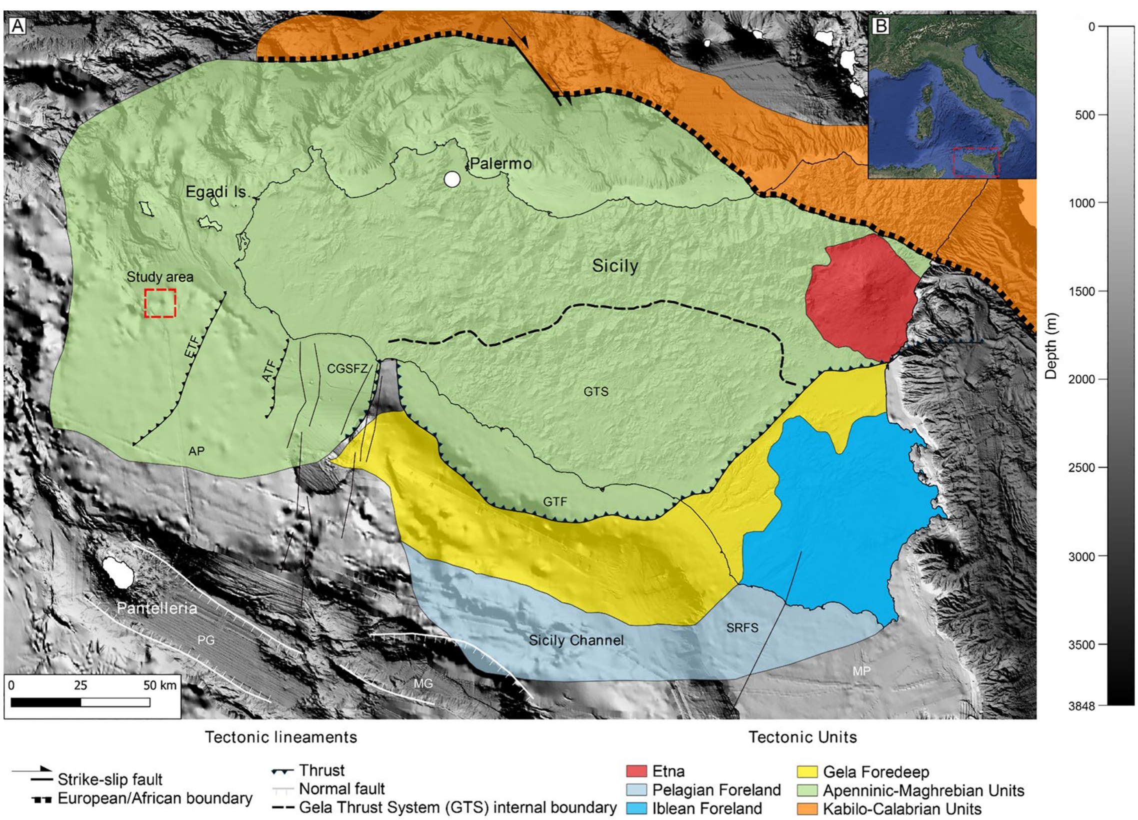

Fig. 1 Inset A shows the bathymetric map with the main and structural elements modified after Gasparo Morticelli et al. (2015), Civile et al. (2018), and Sulli et al. (2021). AP: Adventure Plateau; ATF: Adventure Thrust Front; ETF: Egadi Thrust Front; GTF: Gela Thrust Front; GTS: Gela Thrust System; MG: Malta Graben; MP: Malta Plateau; PG: Pantelleria Graben; SC: Sicily Channel; CGSFZ: Capo-Granitola Sciacca Fault Zone; SRFS: Scicli-Ragusa Fault System. This map also shows the localization of the study area with a red dashed box. Inset B shows the geographical localization of Sicily Island. Source data: EMODnet (https://emodnet.ec.europa.eu/en)

In this paper, we document a large number of pockmarks located near different types of structures that may act as pathway for vertical fluid migration. The study, based on different geophysical datasets, aims (i) to delineate the fluid flow systems on the Adventure Plateau, (ii) to propose a potential origin, and (iii) to improve our general understanding of fluid flow focusing on terms of structural and stratigraphic controls.

Geological background

Geological setting

The Sicily Channel is a shallow marine region between Sicily and Africa with a large and gently sloping (generally less than 1–2°) continental shelf, where the shelf break is located at depths between ~ 100 m in the central part and ~ 150 m along the Adventure Plateau and Malta Plateau (Fig. 1) (Todaro et al. 2022, 2021). The Sicily Channel hosts several morphologies as ridges, volcanoes (e.g., Nerita and Graham banks, Pantelleria and Linosa islands) and deep basins (e.g., Pantelleria, Malta and Linosa grabens) (Figs. 1, 2).

The Adventure Plateau (Figs. 1, 2) has a maximum depth of ~ 150 m and is separated from Sicily by the NW–SE trending Mazara Channel that, towards the north, joints into the Marettimo Channel and the Egadi Valley (Fig. 2), two elongate incisions occurring respectively east and west of Marettimo Island (Fig. 2). The stratigraphic sequence is characterized by a thick Triassic–Eocene carbonate succession (Civile et al. 2014). In the Neogene, the post-collisional convergence between Africa and Europa plates caused the emplacement of the Sicilian Maghrebian Fold and Thrust Belt, which is composed of different tectonic units (Gasparo Morticelli et al. 2015; Sulli et al. 2021). These are characterized by (Fig. 1): – the Pelagian-Iblean foreland with its African crust; – a Late Pliocene–Quaternary narrow foredeep, called Gela Foredeep (GF); – a complex, south to southeast-vergent Fold and Thrust Belt. Along the south-western offshore the main structures of the Fold and Thrust Belt are the Egadi Thrust Front (ETF) and the Adventure Thrust Front (ATF) (Catalano et al. 1996; Fig. 1), while the frontal wedge is called Gela Thrust System (GTS, Fig. 1). The boundary between this accretionary wedge

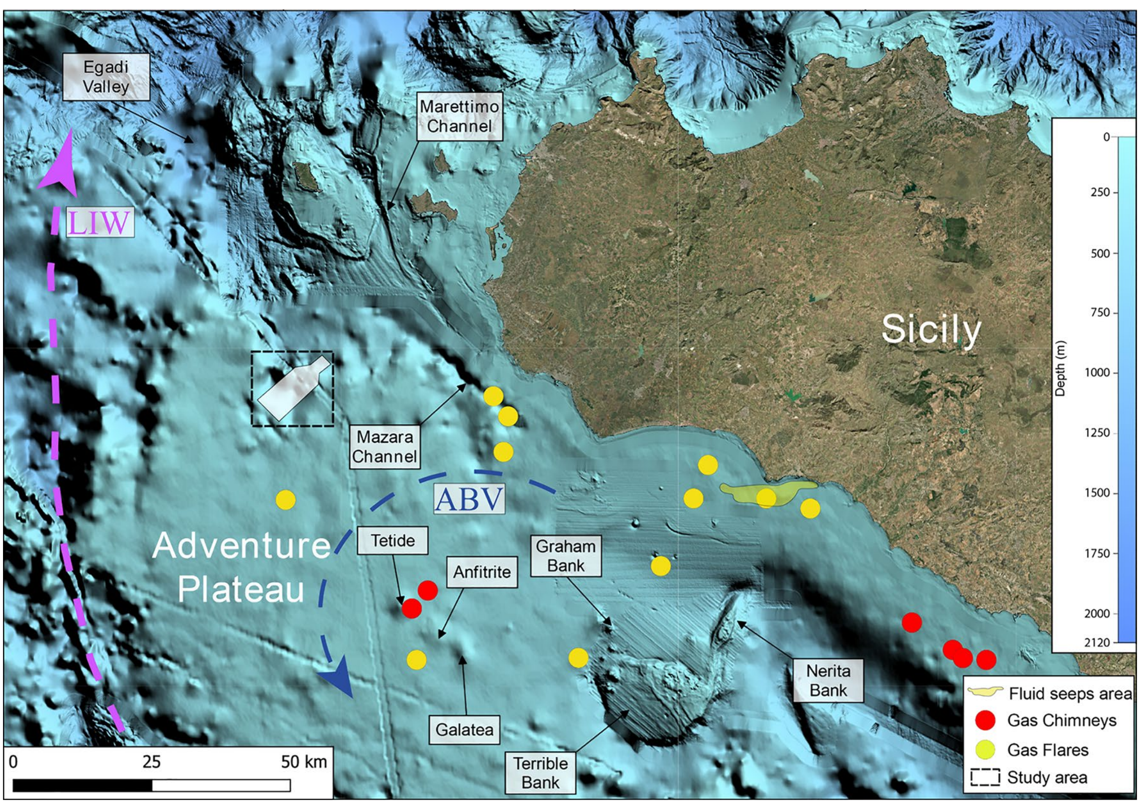

Fig. 2 Bathymetric map showing the main morphological elements from Aissi et al. (2014); the main fluids emission centres from Spatola et al. (2018a) and the fluid seeps area from Civile et al. (2023) the Adventure Bank Vortex (ABV, blue arrow) from Fortibuoni et al. (2010); and the Levantine Intermediate Water (LIW, brown arrow) pattern from Santinelli et al. (2015). Source data: EMODnet (https://emodnet.ec.europa.eu/en)

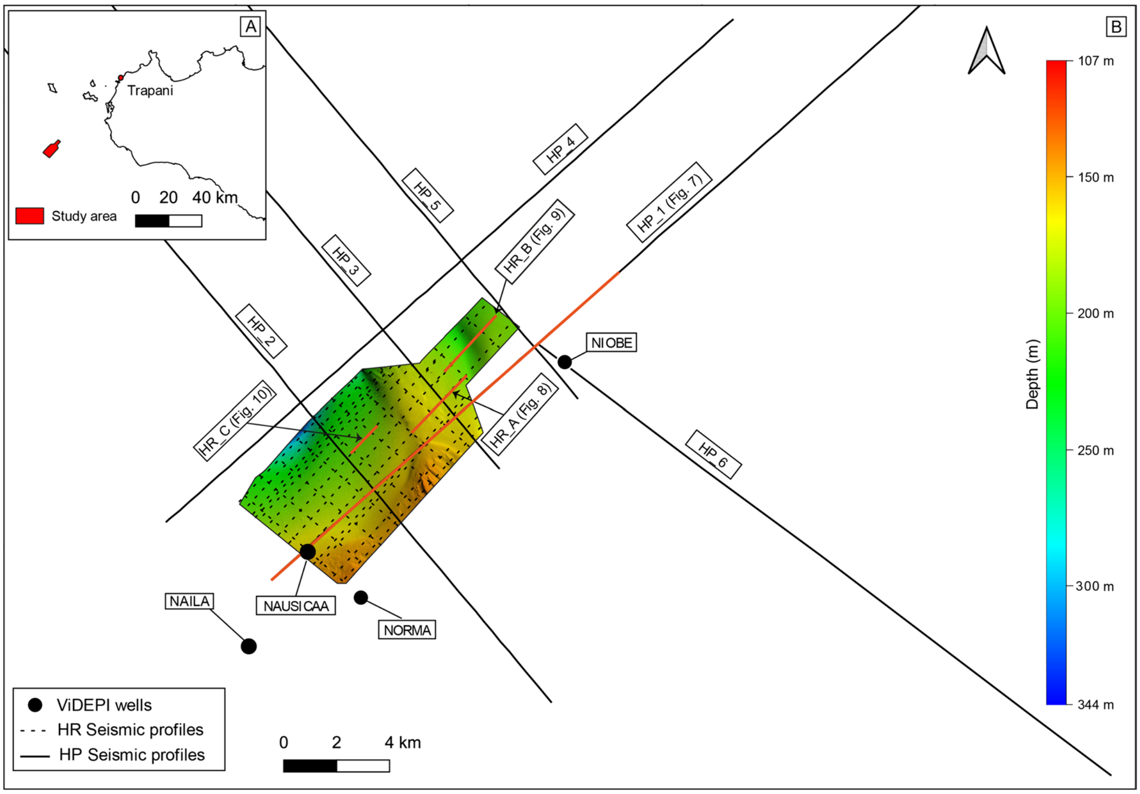

Fig. 3 Study area location (A); coverage map of the dataset used (B): HR (High Resolution) seismic reflection profile, HP (High Penetration) seismic reflection profile, which comprises ViDEPI G (HP_1-5) and LS-89–04 (HP_6) seismic lines, ViDEPI wells, and bathymetric data. Segments of the profiles in related figures are indicated in red

Table 1 Summary of processing sequence for HR seismic data

Application order	Processing steps
1	Band pass filter 20 Hz
2	Despike
3	Source and receiver deghost
4	Reflection coefficient inversion
5	Velocity analysis at 500 m interval
6	Stacking
7	Post stack time migration
8	Post-migration processing
9	Reference frequency 1000 Hz
10	Time Variant Filtering (200 Hz/36 dB – 1600 Hz/36 dB)

and the GF is represented by the Gela Thrust Front (GTF) (Fig. 1) (Gasparo Morticelli et al. 2015). The area has been characterized in the Early Pliocene by a regional extensional event that formed Malta, Linosa and Pantelleria grabens (Fig. 1) (Catalano et al. 1993; Gardiner et al. 1995; Corti et al. 2006; Civile et al., 2021). Today, a mild contractional phase is affecting the Sicily Channel area, in particular the Malta and Linosa Graben (Maiorana et al. 2023), which, in further evidence of northern Sicily compressional phase, suggests a regional plate reorganization and potential subduction polarity switch north of Sicily (Zitellini et al. 2020; Sulli et al. 2021; Loreto et al. 2021). In the Plio-Pleistocene high-angle extensional faults, mainly NW–SE oriented, have modified the original structural setting of this area (Gasparo Morticelli et al. 2015; Parrino et al. 2023). The Adventure Plateau hosts some small and isolated positive reliefs formed of sedimentary or volcanic rocks with different age (e.g., Tetide, Anfitrite and Galatea in Fig. 2) (Civile et al. 2014, 2016).

Recent studies highlighted the occurrence of gas flares and gas chimneys (Fig. 2) by using high-resolution geophysical data testifying active fluid flow systems all over the Sicily Channel such as in the Adventure Plateau, Graham Bank (Coltelli et al. 2016; Spatola et al. 2018b; Ferrante et al. 2022; Volpi et al. 2022; Civile et al. 2023) and Malta Plateau (Micallef et al. 2011, 2019; Savini et al. 2009).

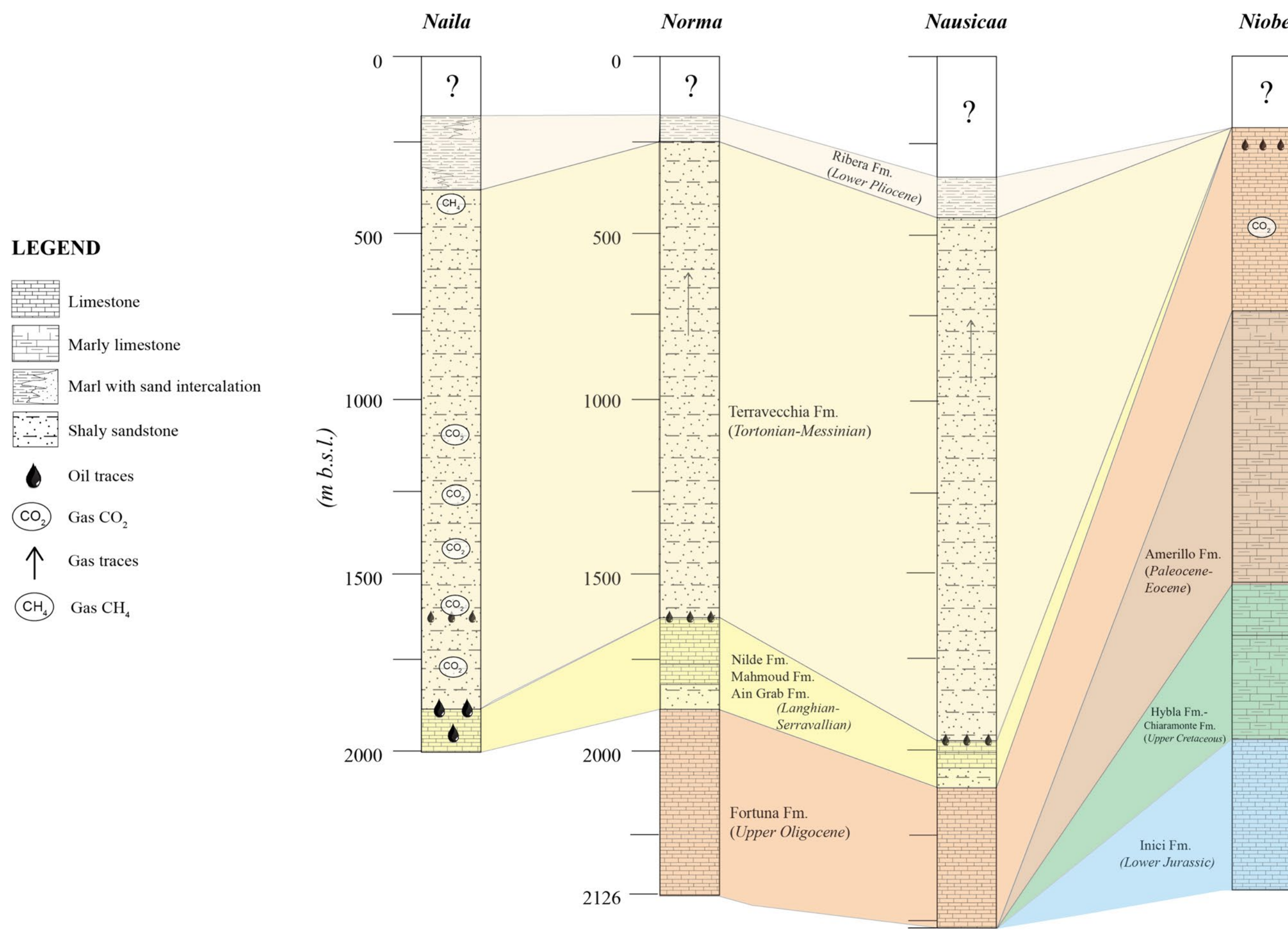

Fig. 4 Stratigraphic correlation table between wells Naila, Norma, Nausicaa and Niobe (location in Fig. 3) in the study area

Oceanographic setting

In the Mediterranean region, the water exchange is represented by a two-layer model which comprises: (i) the MAW (Modified Atlantic Water), a relatively fresh water of Atlantic origin, that flows eastward into the eastern Mediterranean; (ii) the LIW (Levantine Intermediate Water), a salty water formed in the eastern Mediterranean during winter that flows out as an undercurrent into the western Mediterranean (Garcìa Lafuente et al. 2002). The MAW is a shallow current that is partly controlled by topographic features, coastal geometry, and thermohaline boundary forcing. In the Adventure Plateau is divided into two branches: one with a trend towards SE, and the second one that rises towards the NW following an anti-clockwise gyre that is established between Sicily and Sardinia (Istituto idrografico della Marina. Gênes, 1982). The path of MAW varies seasonally with the onset of a large cyclonic eddy (Béranger et al. 2004; Robinson et al. 2001) over Adventure Plateau, called Adventure Bank Vortex (ABV) (Fig. 2). The northern branch, called the Atlantic Ionian Stream (AIS), contributes to the MAW transport into the eastern Mediterranean off the southern coast of Sicily. The Levantine Intermediate Water (LIW) constitutes the main source of water that outflows across the Gibraltar Strait as Mediterranean Outflow Water. It is a deep current (usually confined at a depth between 150 and 600 m) that comes from the Ionian Sea and flows westward crossing the channel south of Malta, occupying the lower part of the water column (around 250–400 m) (Lermusiaux and Robinson 2001; Gasparini et al. 2005; Incarbona et al. 2008; Gauchery et al. 2021). In the western edge of the Adventure Plateau, it flows following a NW-trend and, in the proximity of the Egadi islands, it turns towards the Tyrrhenian Sea (Fig. 2) (Incarbona et al. 2008; Santinelli et al., 2015).

Materials and methods

Seismic data

This study is based on the interpretation of seismic reflection profiles calibrated with well-log data and bathymetric data (Fig. 3). Seismic reflection data comprise variable resolution and penetration profiles. High-Penetration (HP) multi-channel seismic profiles made available through ViDEPI project, were acquired using an airgun as seismic source with a sampling interval of 4 ms (250 Hz), a 6–7 s recording window. Well-log data used for well-tie derived from ViDEPI database as well (Fig. 3). These data were integrated with a high-resolution (HR) seismic grid (Fig. 3) acquired with Dura-Spark sparker as seismic source equipped with 48-channels (150 m long) digital seismic streamer and a 3.125 m hydrophone group interval. The data has a dominant frequency of 1 kHz, resulting in ~ 0.4 m vertical resolution for thin beds. Tab. 1 presents the final processing sequence applied to the HR seismic data.

The seismic interpretation was carried out using the software IHS Markit Kingdom Suite 2021, while the seismo-stratigraphic and structural analysis was performed using MOVE 2022.1 software.

Stress analysis

To identify the leakage zones along faults, following the methodology proposed by Mattos et al. (2016), we evaluated the Leakage Factor (LF) through the tool "Stress Analysis" (MOVE 2022.1). The Stress Analysis Module allows the colour-scaled 3D visualization of the fault planes that are more likely to reactivate and leak. This method was applied along the main structural element of the study area which was identified by the seismo-structural interpretation supported by HP data.

The leakage factor (LF) is (for each geometric portion of the fault plane) the ratio between the pore pressure (Pp) and the difference between the normal stress (σn) and the shear stress (τ):

$$LF : Pp/(\sigma n - \tau)$$

Leakage factor (LF) allows the quantitative modelling of the fluid transmissivity of faults, identifying faults that either constitute migration conduits for sub-surface fluid or, instead, act as local seals (Mattos et al. 2016). It has been calculated based on the actual stress field of the study area considering: $\sigma n = 203\ \mathrm{N/m^2}$; $\tau = 123\ \mathrm{N/m^2}$ (data from https://www.world-stress-map.org/), and the Pp = 1.5 MPa (data from Niobe well-log).

***Morpho*-bathymetric data**

Bathymetric data have been acquired through MBES system by using a Teledyne SeaBat T50-P, with a differential Global Positioning Systems. These data were processed using the CARIS HIPS and SIPS v.10.4 software and entailed removal of erroneous beams, noise filtering, calibration and processing of navigation and correction for sound velocity. The derived Digital Terrain Model (DTM) has a bin size of 0.5 m. The interpretation of the Multibeam Echosounder (MBES) data (Fig. 3) was performed with Global Mapper (https://www.bluemarblegeo.com/global-mapper/) software to identify and map key

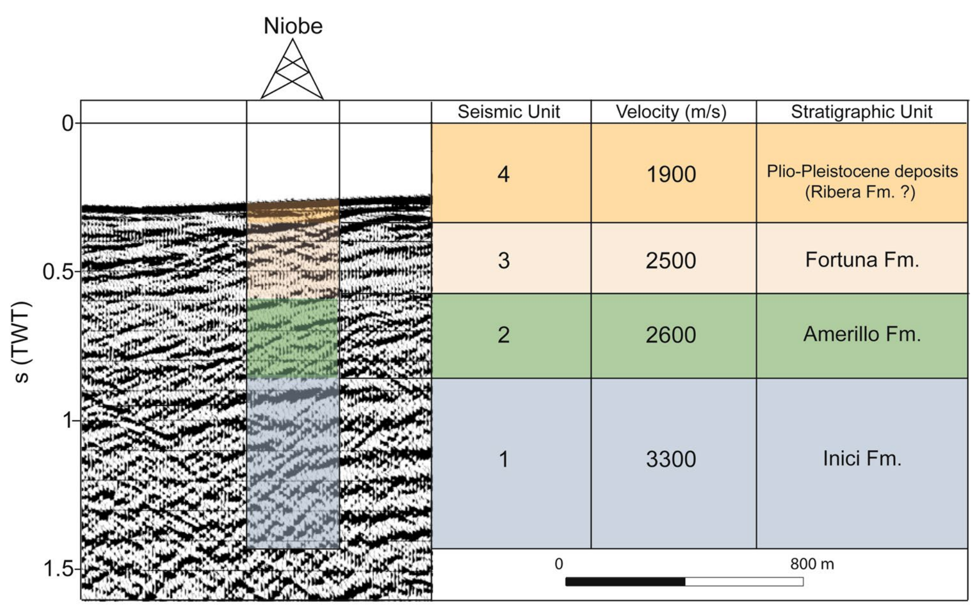

Fig. 5 Stratigraphic succession of the Niobe well-log used to calibrate seismic facies units 1–4 in the HP_1 seismic profile. Next to the units are shown the seismic velocities values used for conversion from m to s (TWT) of the main stratigraphic levels

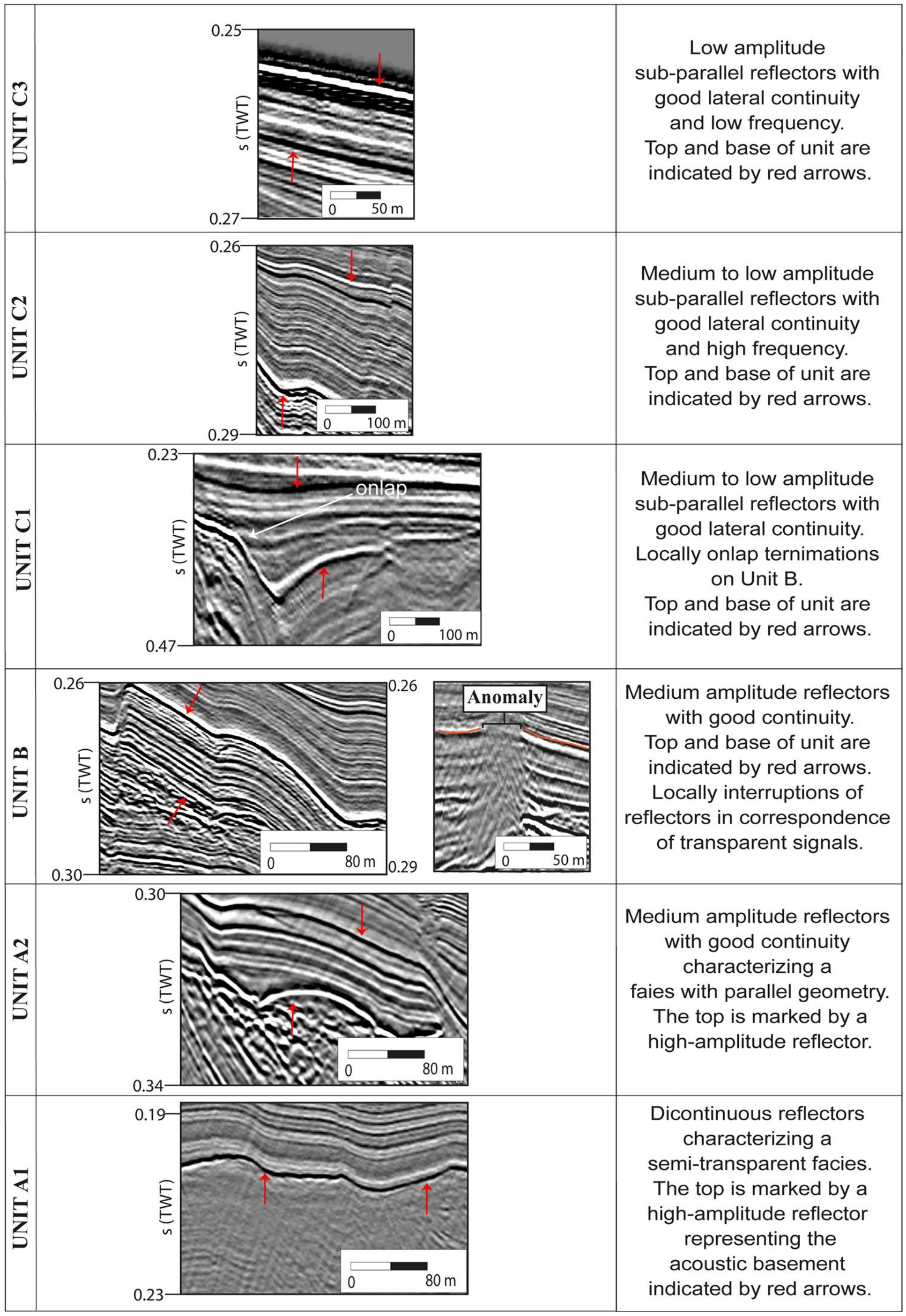

Fig. 6 Seismic units identified by the seismo-stratigraphic analysis of HR seismic reflection profiles

seabed morphological features associated with fluid flow phenomena, such as pockmarks.

Morphometric analysis

The morphometric characterization of the pockmarks was performed using the semi-automatic method for extracting the main parameters and applied for the first time to study pockmarks around the Ferdinandea Island (Sicily Channel) by Spatola et al. (2023). In this study, authors modified methodologies applied for submarine volcanoes in the Tyrrhenian Sea (Sulli et al. 2020), in the Canary Islands (Ruiz et al. 2000), and in the Sicily Channel (Cavallaro and Coltelli 2019; Spatola et al. 2018b).

The pockmarks boundaries have been manually identified mapping the sharp breaks in slope, recognised in the cross-section profiles from the 0.5 m resolution DTM. This method was used to calculate both their basal surface and different

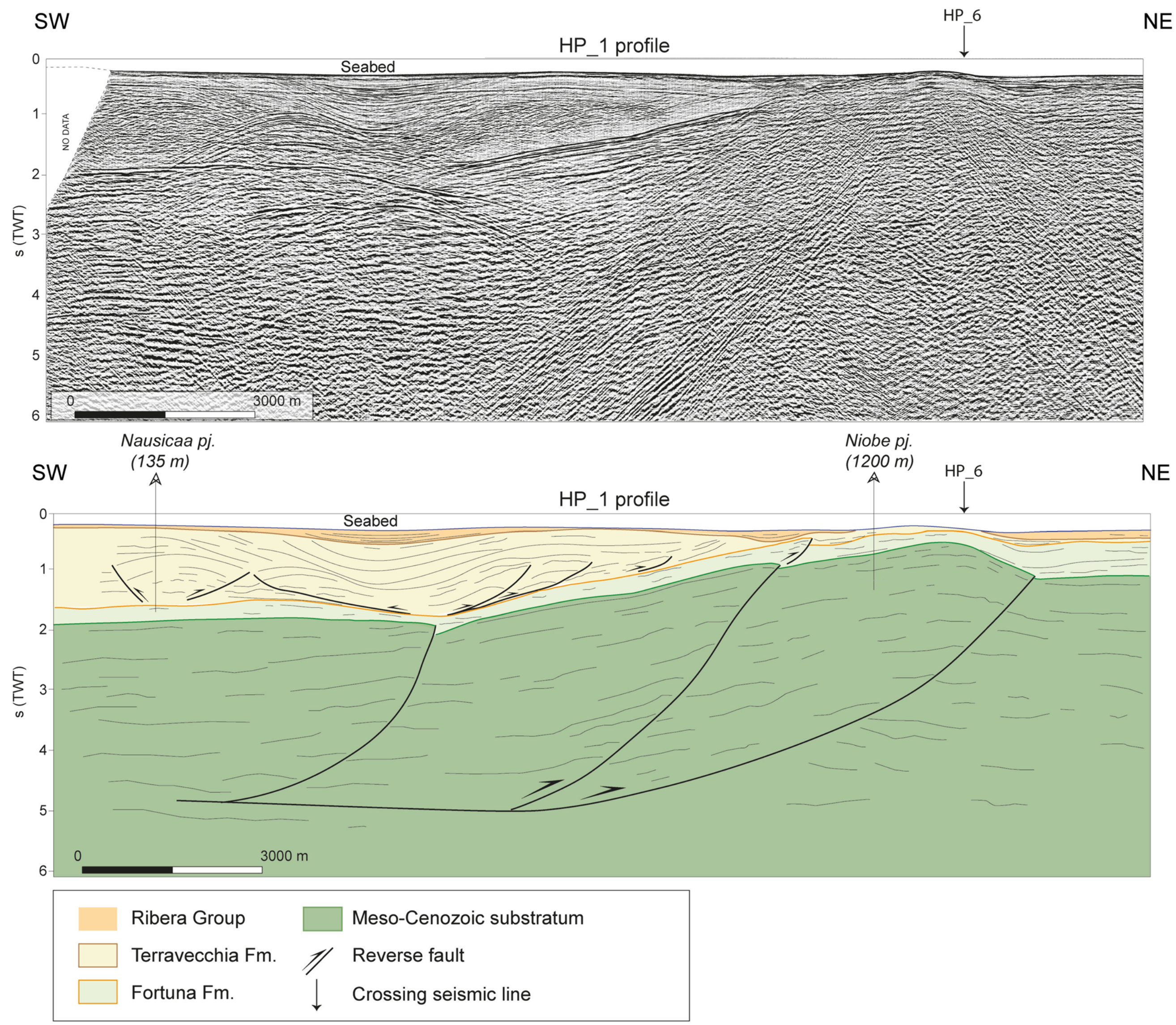

Fig. 7 Line drawing of the HP_1 seismic reflection profile (location in Fig. 3) showing the deep structural framework of the study area

geometrical parameters (e.g., major, minor, and mean axis). We also measured other parameters according to Grosse et al. (2009, 2012), such as:

1) "di" dissection index ($di = (Perimeter/2*Surface)*(\sqrt{(Surface/\pi)})$). It quantifies the irregularity or complexity of the pockmark, relating the perimeter with the enclosed area.
2) "ei" ellipticity index ($ei = (\pi*(Major\ Axis/2)^2)/Surface$). It quantifies the pockmark's elongation relating the length of the main axis with its area.
3) "e" eccentricity ($e = (\sqrt{(Major\ Axis/2)^2\text{-}(Minor\ Axis/2)^2}/Major\ Axis/2)$). It defines if the pockmark shape tends to be circular ($e = 0$), or elliptical relating to the pockmark's major and minor axes.

The last two indexes are two different options to define the same characters of the external shape of different kinds of morphologies. In this paper, we prefer to use both since they are used indifferently in the recent literature (Gafeira et al. 2012; Grosse et al. 2012).

Results

Well-log analysis

A well-log analysis has been carried out through a stratigraphic correlation (Fig. 4) among the well-logs of Naila, Norma, Nausicaa and Niobe wells (location in Fig. 3), available from ViDEPI database (source https://www.videpi.com/videpi /videpi.asp). This analysis highlighted the variability of the pre-Pleistocene substrate in the study area: in fact, it is possible to recognize the transition, from SW to NE, from the Lower Pliocene (Ribera Fm.) to the upper Oligocene (Fortuna Fm.) and so, the absence of the outcropping Pliocene units in the NE sector of the area.

Gas and oil traces have been detected in all the stratigraphic well-logs (Fig. 4), respectively in:

- Niobe well-log, showing the presence of oil traces at a depth of 250 m b.s.l., and gas (CO_2) at a depth of 500 m b.s.l., within the Fortuna Fm.;
- Norma well-log, showing oil traces from 1660 to 1676 m b.s.l. at the top of the Nilde Fm. and gas traces of undefined composition inside the Terravecchia Fm.;
- Nausicaa well-log, showing oil traces between 1948 and 1950 m b.s.l. at the top of the Nilde Fm. and gas traces of undefined composition inside the Terravecchia Fm.;
- Naila well-log, showing oil traces between 1885 and 1910 m b.s.l. at the top of the Nilde Fm. and gas (CO_2) between 1110 and 1875 m b.s.l..

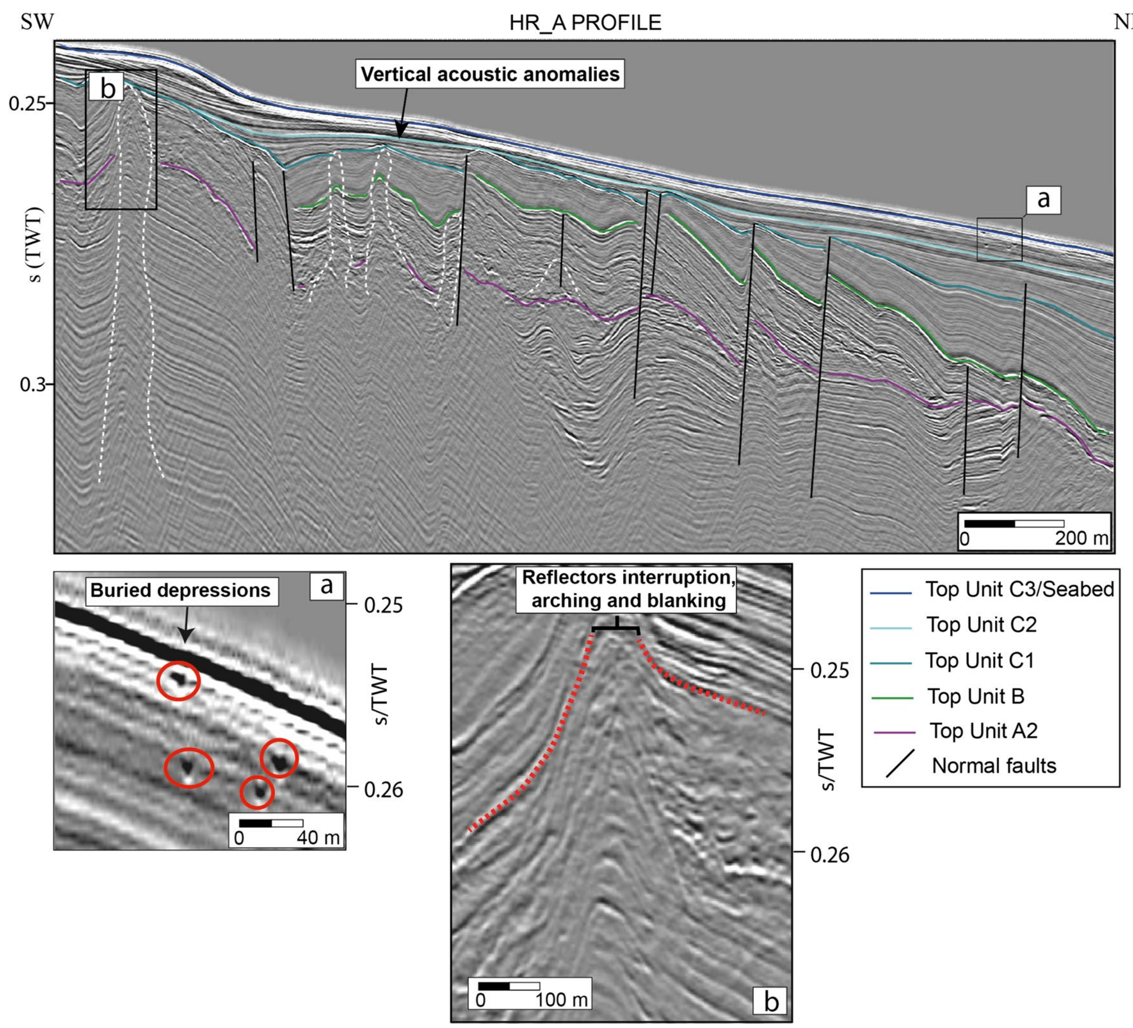

Fig. 8 HR_A profile (location in Fig. 3) showing the presence of vertical acoustic anomalies (white polygons) occurring with a vertical arching of the reflectors. Inset (a) shows the occurrence of buried depression; inset (b) shows a zoom of reflectors arching, interruption and blanking

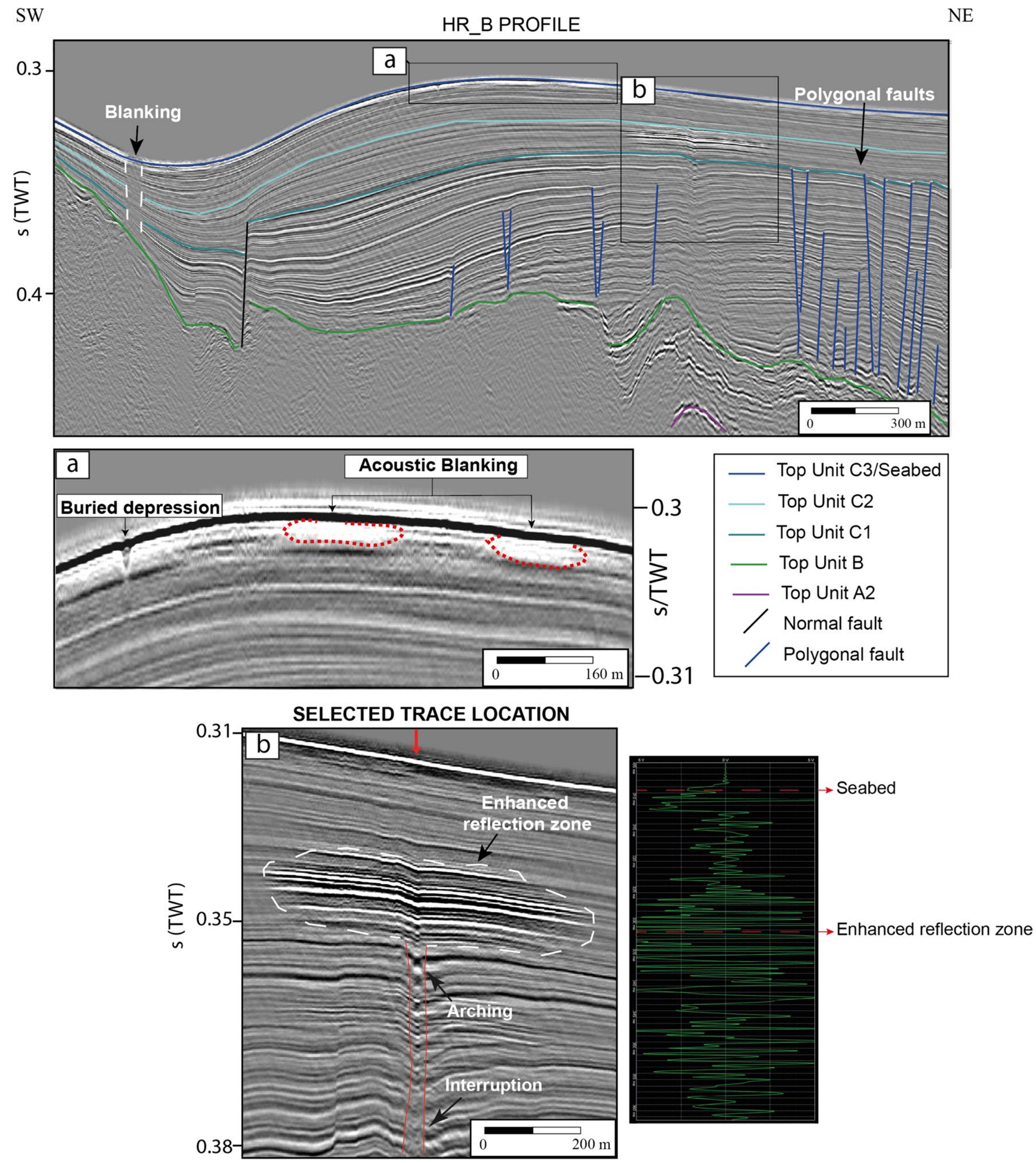

Fig. 9 HR_B profile (location in Fig. 3) showing the occurrence of wide vertical acoustic anomaly topped by an enhanced reflection zone. In the SW sector, an acoustic blanking is also observed. The inset (a) shows a detail of a shallow buried depression and two acoustic blanking zones. In the inset (b), on the left, the zoom of the enhanced reflection zone and the vertical acoustic anomaly is visible; on the right, the upper part (from 0.31 to 0.38 s (TWT) of the seismic trace is shown

Seismo-stratigraphic and structural analysis

The joint analysis of seismic data of variable penetration allows us to identify the corresponding seismic units between the two different dataset and to characterize the presence of deep and shallow anomalies potentially related to a fluid occurrence.

High Penetration seismo-stratigraphy and well-tie

A seismo-stratigraphic analysis has been carried out to identify the seismic units of the HP seismic profiles (location in Fig. 3). The well-tie has been performed using sonic log data to obtain velocities for a depth-to-time conversion (Fig. 5).

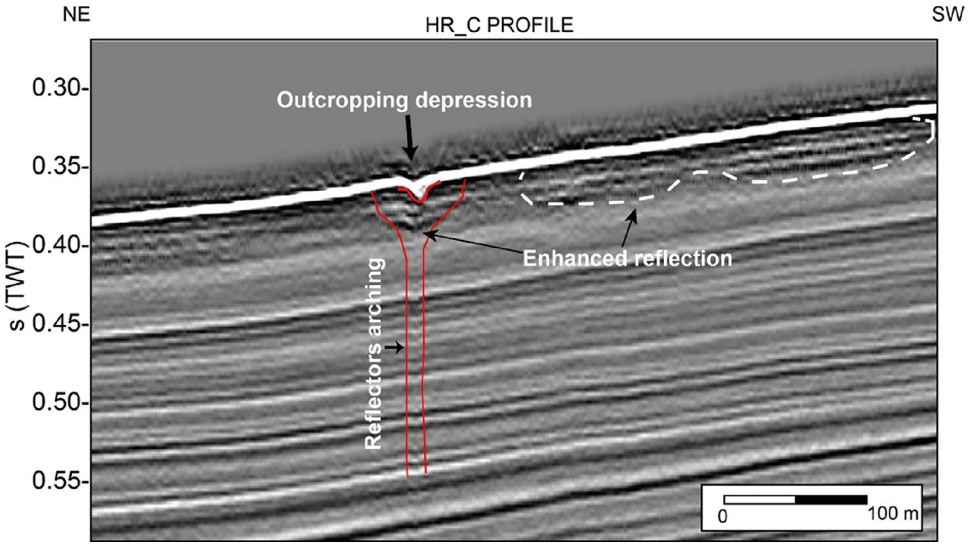

Fig. 10 HR_C profile (location in Fig. 3) shows the occurrence of an outcropping depression limited to the base by an enhanced reflection zone, also extending laterally in the SW sector of the profile. A vertical acoustic anomaly (downward arching of reflectors) develops from 0.55 s (TWT) to the base of the depression

We identified 4 different units named from 1 to 4, starting from the bottom (Fig. 5).

- The seismic unit 1 shows low-frequency and high-amplitude reflectors. This has been attributed, through the well-tie process, to the Inici Fm. (Fig. 5).
- The seismic unit 2 shows, a medium frequency and amplitude of the reflectors, that has been attributed to the Amerillo Fm.
- The seismic unit 3 is characterized by discontinuous and semi-transparent facies and has been attributed to the Fortuna Fm.
- The overlying unit 4, shows high frequency and a plan-parallel geometry of reflectors, with low amplitude and good lateral continuity, The latter has been attributed to the Plio-Pleistocene deposits, not registered in Niobe well-log, but laterally correlated by Nausicaa well-tie (Fig. 5), and therefore attributed to the Ribera Fm.

High resolution seismo-stratigraphy

The seismic facies analysis of the HR seismic reflection profiles highlighted the occurrence of three main seismic units (A, B, C) and five sub-units (A1, A2, C1, C2 and C3) (Fig. 6), as follows:

Unit A: the lowest unit recognized in the HR seismic profiles was divided in two sub-units, respectively Unit A1 and A2. Unit A1 is characterized by a high amplitude reflector representing the acoustic basement, which is the bottom reflector of Unit A2. The latter is characterized by semi-transparent facies with parallel reflectors. Its top limit is marked by a high amplitude reflector.

Unit B: it is characterized by low amplitude reflectors with medium frequency. Locally anomalies characterized by interruptions of reflectors are observed in correspondence of transparent signals.

Unit C: it consists of medium to low amplitude sub-parallel reflectors with good lateral continuity, affected by several faults. Unit C is composed by three sub-units (C1-3); Unit C1 shows onlap lateral terminations on the unit B, C2 (with high frequency of the reflectors) and C3 shows an upward progressive diminution of amplitude and frequency of reflectors.

High penetration seismic reflection profiles interpretation

The analysis of high-penetration seismic reflection profiles enables the comprehension of the deep structural geometry and the identification of pathways for deep-seated fluid migration within the study region.

The seismic profile HP_1, crossing the study area from NE-SW, for its proximity, has been calibrated by projecting of the closely located Niobe (1200 m far) and Nausicaa (135 m far) well-logs. A NE-vergent thrust dissects layers from 5 to 1 s (TWT) has been identified, involving the Inici, Amerillo and Fortuna Fms, in agreement with compressional tectonics mapped by Milia et al. (2021) in the same area and with the LS-89–04 seismic line (HP_6 in Fig. 3) interpreted and available in the ViDEPI database. This main thrust surface turns out to have a Leakage Factor (LF) of 1.5 which suggests a high permeability potential. In the southern sector, a significative filling, 1.8 s (TWT) of the thrust top basin is observed (Fig. 7); this, accordingly to the Nausicaa well-log, comprises respectively the Terravecchia Fm. and the Ribera Fm. (Fig. 7). Inside the basin (filled by Terravecchia Fm.) several thrusts have been observed (Fig. 7); those appear detached from the underlying level (Fortuna Fm.) and sealed by the parallel deposits of the

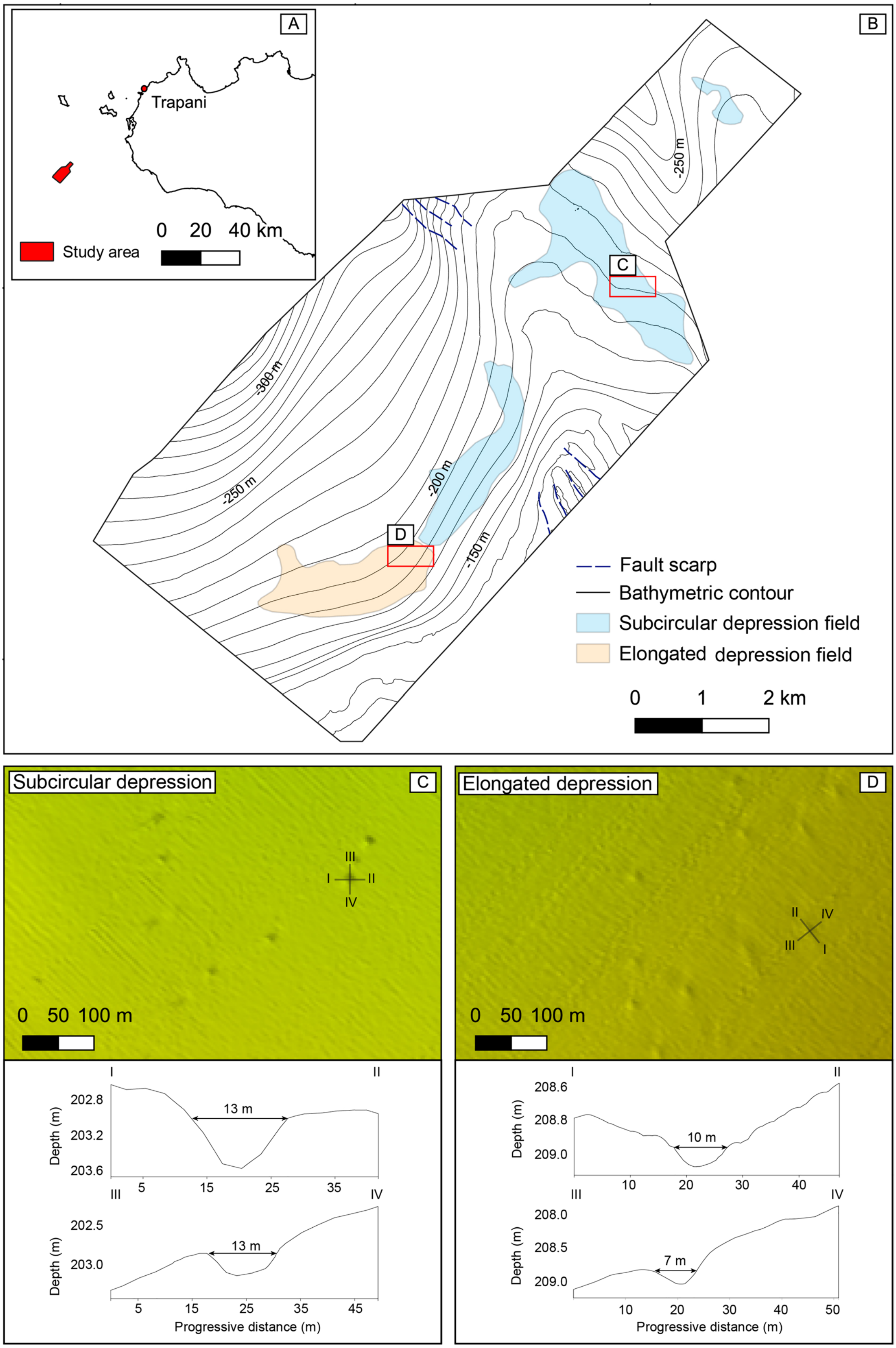
A
Trapani
0 20 40 km
Study area
B
-250 m
C
-300 m
-250 m
-200 m
D
-150 m
Fault scarp
Bathymetric contour
Subcircular depression field
Elongated depression field
0 1 2 km
Subcircular depression
C
0 50 100 m
Elongated depression
D
0 50 100 m
Depth (m)
202.8
203.2
203.6
13 m
5 15 25 35
202.5
203.0
13 m
5 15 25 35 45
Progressive distance (m)
208.6
208.8
209.0
10 m
10 20 30 40
208.0
208.5
209.0
7 m
10 20 30 40 50
Progressive distance (m)

◂**Fig. 11** Study area location (A); the inset (B) shows the geomorphological chart of the study area in which are represented the bathymetric contours (black lines), the fault scarp (blue dashed line), the subcircular pockmark filed (light blue polygons) and the elongated pockmark field (light orange polygon). Inset C and D show the depressions on the high-resolution DTM with 2 perpendicular bathymetric profiles

Ribera Fm. Thus, a secondary compressive phase from post-Oligocene to Lower Pliocene is highlighted in the study area (Civile et al. 2014).

High resolution seismic reflection profiles interpretation

New constraints on the stratigraphic setting of the shallower levels in the study area show an alternation of different layers located inside the Ribera Fm. Further, the evidence of vertical acoustic anomalies (e.g. gas chimneys sensu Hustoft et al. 2010), horizontal acoustic anomalies and buried and/or outcropping depressions, all generally associated with fluids indicators (Judd & Hovland 1992, 2007), prove the occurrence of fluids at shallow layers. The identified vertical acoustic anomalies in the area present three different seismic characters: the first one shows clear enhanced reflections, the second one is characterized by blanking areas and the last one shows clear reflectors arching; anomalies showing these all three seismic characters are indicated as gas chimneys similar to those mapped in the north-western Sicily Channel (Fig. 2; Spatola et al. (2018a). The identified horizontal acoustic anomalies in the area present two seismic characteristics: acoustic blanking and enhanced reflections. The latter shows a strong increase in seismic amplitude, with reversed polarity compared to the seafloor reflection (Fig. 9b). This evidence has been linked to an abrupt change in the elastic properties of the sedimentary sequence, attributed to the presence of gas by many authors (Gay et al. 2007; Tinivella et al. 2009; Pennino et al. 2014).

Normal faults, cutting across units A2 to C1, are sealed by the subunits C2 and C3 (Figs. 8, 9) and are accompanied by the presence of vertical seismic anomalies; those appear as both concave or convex reflectors and are characterized by semi-transparent facies. These seismic characteristics, which have high similarity with those recognized in the nearby Graham Bank by Spatola et al. (2018b), have been interpreted as seismic chimneys. Thus, these faults represent a conduit for vertical fluid migration only within the A-C1 units, not exhibiting fluid escaping to the seafloor.

The HR_B profile shows also the presence of gas chimneys within Units B to C interrupted right below an enhanced reflection zone (Fig. 9). The seismic trace, which highlights the P wave recorded as amplitude peaks in the water column, was extracted along the enhanced reflection zone (horizontal acoustic anomaly), highlighting a signal inversion at the top of the anomaly (Fig. 9b).

HR_C profile shows the occurrence of an outcropping depression limited to the base by a horizontal acoustic anomaly characterized by an enhanced reflection zone, extending laterally from the depression to the SW sector of the profile (Fig. 10). Another vertical acoustic anomaly, characterized by a downward arching of reflectors, has been detected from 0.55 s (TWT) to the base of the depression itself.

Analyzing the HR seismic dataset, a total of 15 vertical acoustic anomalies and 10 horizontal acoustic anomalies have been mapped. These are often associated with sub-vertical discontinuities mainly affecting Unit C2 that is characterized by complex kinematics, with throws between 5 to 20 m and small spacing of up to 500 m, therefore interpreted as polygonal faults (Berndt et al. 2012). In this unit, different enhanced reflections have been identified (Fig. 9). Right beneath the seafloor, in Unit C3, we observed the presence of acoustic blanking zones (Fig. 9a) and some buried depressions (Fig. 8a; Fig. 9a). In the whole area 20 acoustic blanking zones were identified. Assuming a sound velocity of 1500 m/s the width of this anomaly ranges from 50 to 180 m and the heights from 10 to 15 m. The identified 5 enhanced reflection zones appear extended laterally in a NW–SE direction for about 800 m.

Morpho-bathymetric analysis

The bathymetric data covers an area of ~ 80 km^2 with a water depth ranging between 107 and 344 m (Fig. 11). The study area is characterized by the presence of a structural high, evident from the bathymetric contours on the NE sector of the study area (Fig. 11B) oriented NNW-SSE with a height of about 40 m. Faults scarps of 20 m high, occupy respectively the southeasternmost and northwesternmost sectors of the study area. The bathymetric contours show an increasing depth towards NW, from ~ 140 m to ~ 340 m, due to the presence of a morphologically depressed sector

Table 2 Measured parameters of mapped depressions in the study area

Depressions	Minimum	Maximum	Mean	Standard deviation
Sumimt depth (m)	165	243	198	13
Basal depth (m)	166	244	198	13
Depth/Radius	0	2.36	0.07	0.15
Flank slope (°)	0	1.52	0.64	0.27
Ellipticity index	0.96	5.82	1.70	0.98
Dissection Index	1.03	7.42	1.34	1.01
Depth/Surface	0.0008	0.14	0.00	0.01
Eccentricity	0	0.98	0.61	0.23

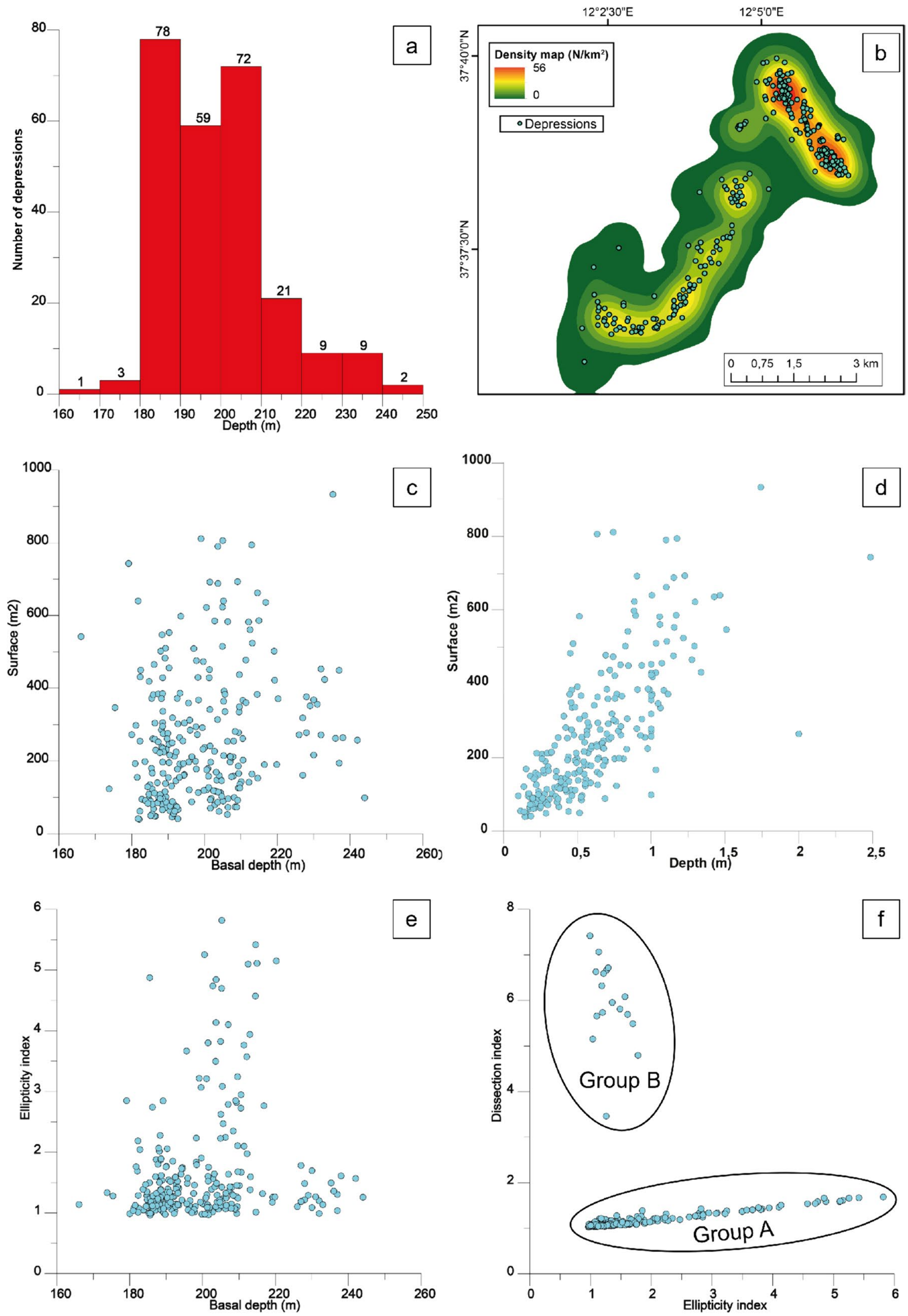

Fig. 12 Summary graphs of the morphometric analysis of the identified depressions

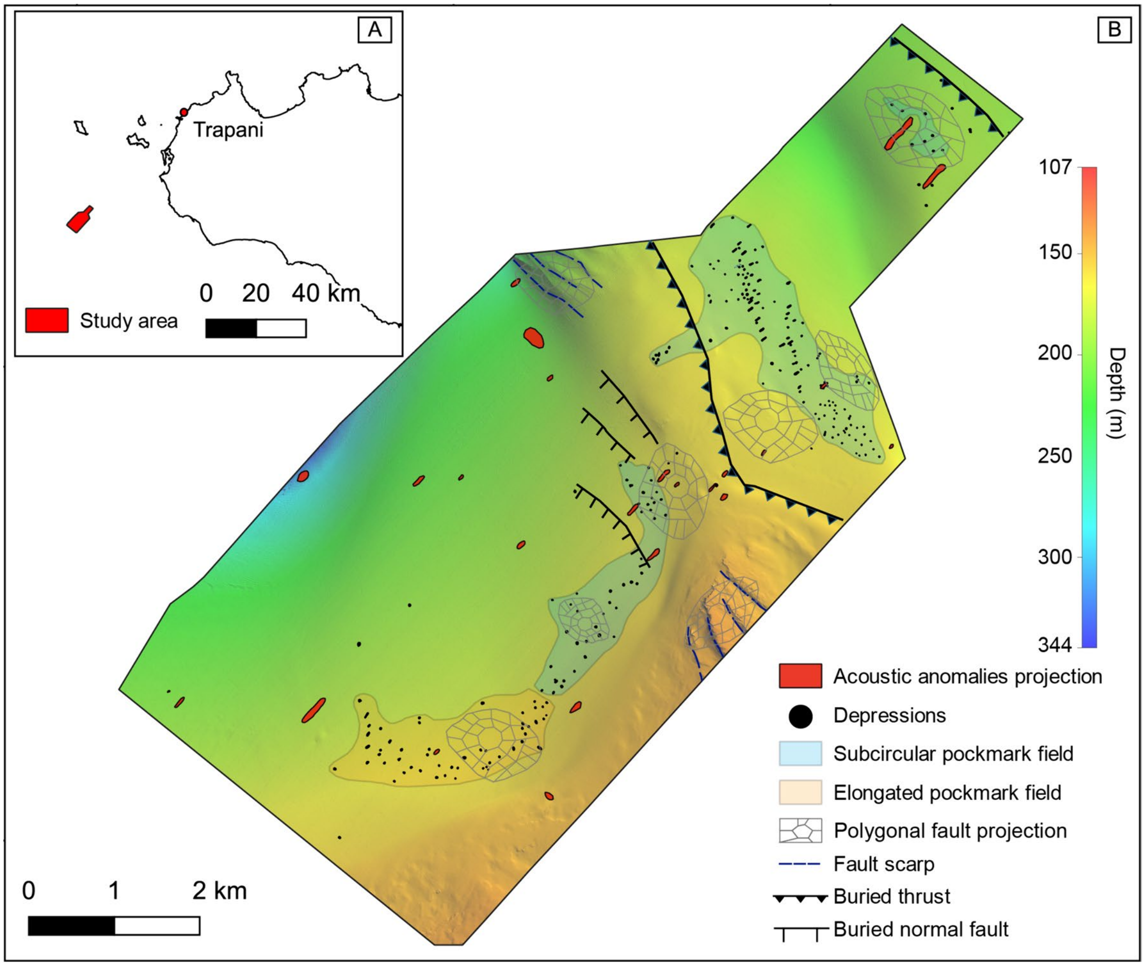

Fig. 13 Study area location (**A**) and high-resolution DTM (**B**) in which are represented the main morphostructural elements. Polygonal fault with a graylish pattern, fault scarp with a dashed blue line, buried thrust with black lines and triangles, buried normal fault with black line, acoustic anomalies projection with a red polygon, pockmark depression with black dots, subcircular pockmark field with light blue polygon and elongated pockmark field with light orange polygon

in the western part of the study area. The seafloor is punctuated by 247 depressions of variable depth, that have been differentiated in ''fields'' based on their morphology. As visible in the Fig. 11, two different types of depressions have been distinguished, subcircular and elongated, that have been grouped into depression fields. Three subcircular depression fields occur in the northern sector of the study area, two showing a NW–SE orientation, and the southern one a NE-SW orientation. In the southern sector of the study area, a NE-SW oriented elongated depression field has been recognized.

Morphometric analysis of depressions

Based on the interpretation of morpho-bathymetric data, we measured and calculated some morphometric characteristics of the identified depressions such as (1) ellipticity index, (2) dissection index and (3) eccentricity (Table 2).

Figure 12 presents summary graphs, including a vertical histogram and scatter plots of the measured parameters. Figure 12a shows the depth distribution of the 247 depressions identified between 160 and 250 m: the most representative depth range is 180 to 220 m. The depressions' density map (Fig. 12b) identifies two main trends: a NW–SE and a NE-SW array, which curves in an E-W direction in the southernmost part. The highest density of pockmarks (56/km^2) is observed in the northern sector and shows a NW–SE orientation.

The graph in Fig. 12c shows that the average depth is mostly less than 1 m, with a surface extension ranging from ~ 50 to ~ 400 m^2.

The surface (m^2) vs. depth (m) graph (Fig. 12d) shows that surface extension increases linearly with the depth of the depressions. Instead, the ellipticity index vs. basal depth (m) graph (Fig. 12e) shows that the ellipticity index remains confined mainly between 1 and 2, indicating that most of

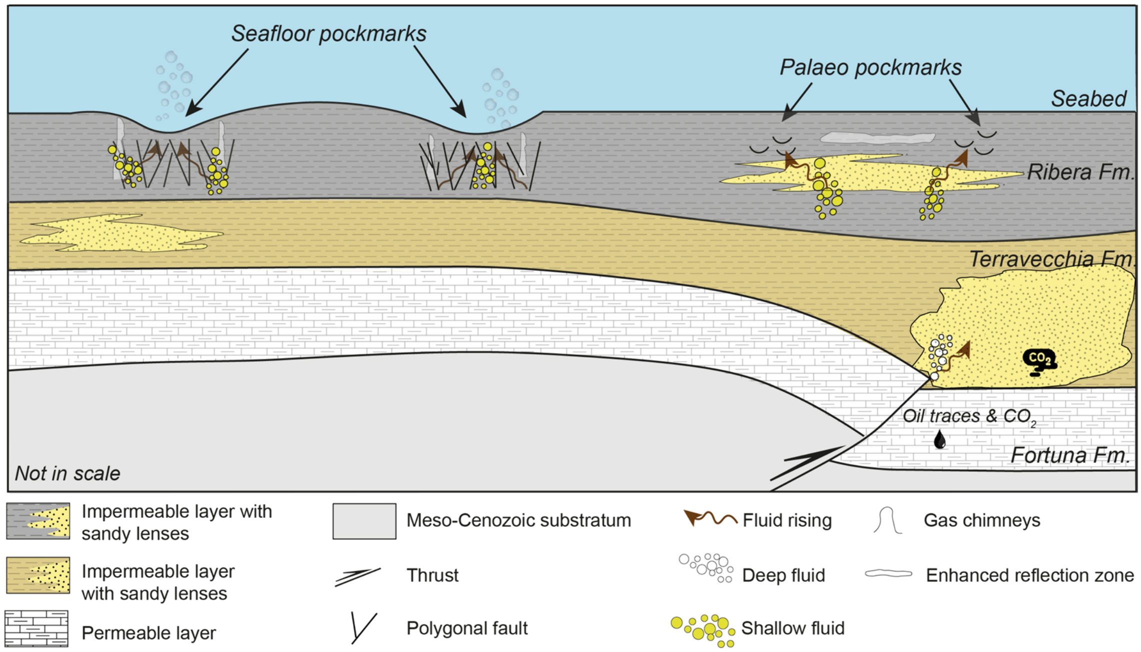

Fig. 14 Fluids rising model of deep and shallow fluids outlined by means of alternate permeable and impermeable layers

the depressions have a subcircular geometry. Finally, the dissection index vs. ellipticity index graph shows that as the ellipticity increases, the dissection index remains almost constant (Fig. 12f). In this graph, two groups of values have been identified. Group A shows an increasing ellipticity index and a constant dissection index, while Group B shows a reverse behavior (Fig. 12f).

Morpho-structural analysis

The main morpho-structural elements of the study area, deriving from both morpho-bathymetric and seismic reflection profile analysis, are summarized in Fig. 13. The seismo-structural interpretation of HP profiles shows the presence of a main buried thrust NW–SE oriented, crossing the study area (Figs. 7 and 13); close to the top of this high, buried normal faults with a NW–SE trend have been identified. Moreover, in the eastern boundary of the study area, several faults' escarpments occur, assuming values ranging from ~ 10 m to ~ 20 m (Fig. 13).

Fields of elongated and subcircular depressions are observed in correspondence with the 25 seismic anomalies identified in the HR profiles. Those are located directly above seismic offsets and fault zones (Figs. 9, 13) and below the outcropping depressions (e.g., Fig. 10). It is also visible how different polygonal faults lie inside the depression's fields, supporting the hypothesis of a correlation between the identified structures and the depressions (Micallef et al. 2019).

Discussions

Fluid flow could be responsible of a wide range of seabed morphological features (Hovland et al. 2010). Among these, pockmarks are often associated with subsurface anomalies e.g., gas chimneys or pipes that acts as pathways through the surface (Cartwright et al. 2007; Løseth et al. 2009).

The well-log data available, highlighted the presence of gas (CO_2 or probably also CH_4), in the Terravecchia Fm., Amerillo Fm. and Fortuna Fm., and the presence of oil traces at high-to-shallow depth within the Fortuna Fm. Through the analysis of different resolution seismic data, we highlighted the occurrence of several acoustic anomalies on the Adventure Plateau at high to shallow depth. Those are characterized by both acoustic blanking areas, enhanced reflections and reflectors arching and their projection corresponds to buried and outcropping depression fields where also polygonal faults projection lies (Fig. 13). The presence of polygonal faults suggests the occurrence of a dewatering and compaction process (Berndt et al. 2012) developing from the host sediment composed of the clays of the Ribera Fm. Such faults, which do not have a tectonic origin (Cartwright et al., 1994), are tightly linked to the basin fluid flow system, as they are generated by pore water expulsion.

Evidence of the occurrence of (i) fluids in the boreholes recorded at different depths, (ii) acoustic anomalies branching to the seafloor, sometimes below outcropping depressions, and (iii) polygonal faults, allowed us to link the detected depressions to fluid escape structures and to interpret them as pockmark. Considering the absence of gas flares from seismic evidence, we assume that they were active in recent times, but are no longer active today.

The identified subcircular and elongated depression fields have therefore been attributed respectively to subcircular and elongated pockmark fields. The highest density of pockmarks occurs in the northern sector, where they follow a NW–SE trend, inside a subcircular pockmark field.

The morphometric analysis highlighted the presence of two main groups of pockmarks in the dissection index versus the ellipticity index graph. Group A shows a linear correlation between dissection and ellipticity index (Fig. 12f): considering the low value of dissection index, indicating regular/smooth edges, and growing values of ellipticity index, we suggest a potential role of the bottom current in the shaping of these fluid flow morphologies. Group A corresponds to the elongated depression field in Fig. 13, reinterpreted as an elongated pockmark field. The elongated pockmark field shows a major axis orientation, orthogonal (NE-SW) to the tectonic trend, so their elongation cannot be attributed to tectonic control. Instead, the NE-SW direction of the elongated pockmark in Group A is in agreement with a potential influence of the ABV; although it is a surface current, given the shallow depth of the seafloor in the study area, we suggest that ABV could have effects on shaping the pockmarks morphology.

Conversely, Group B shows very high values of dissection (irregular edges), and very low values of ellipticity (Fig. 12f) indicating a subcircular morphology that is therefore not affected by the bottom current.

Fluid rising model

The fluid rising model we propose reconstructs the source and the paths of the rising fluids, taking into account the geometry of sedimentary layers and the occurrence of permeable and impermeable layers derived from well-log analysis (Fig. 14).

Based on these observations, two fluid sources were identified in the study area:

The deepest (i), which does not create outcropping fluids emission morphologies, is documented by oil traces and CO_2 contained in the Fortuna Fm. limestone (Fig. 4). The buoyancy generated in the ramp anticline at the hanging wall of the Miocene thrust, induces the migration of the fluids, which rise by advection to the Terravecchia Fm., thanks to the positive LF of the thrust. These fluids are locally confined in small sandy and more permeable lenses of the Terravecchia Fm. (Fig. 14).

The shallowest (ii) is related to biogenic gases formed in the impermeable clay layer (Ribera Fm.) as observed in the Zagara well (ViDEPI), some tens of kilometers to the ENE from this area.

Based on the observed features, we suggest that these shallow fluids migrate by two different mechanisms: (a) dewatering and compaction of sediments confirmed by the polygonal faults presence (Berndt et al. 2012) and focused emissions (e.g., gas chimneys); (b) diffusion through sandy lenses (Fig. 14) that induces the generation of dispersed emissions on the seafloor, as suggested by the presence of broad horizontal anomalies (e.g., enhanced reflections) and paleo pockmarks, similar to those described on the Malta Plateau by Micallef et al. (2011) (Fig. 14).

Conclusions

This study highlights the presence of two different types of fluids: (i) one containing mainly gas, identified at 700–820 m b.s.l., at the boundary between Amerillo Fm. and Fortuna Fm.; (ii) the second one, mainly composed of oil, identified at shallower depth, between 242 and 282 m b.s.l., inside the Fortuna Fm.

Two sources have been identified: one, deeper, unrelated to the surface, the other, shallower, responsible for pockmark formation.

The deeper source derives from the Fortuna Fm., rises through advection in the Terravecchia Fm., and confines in the sandy layers.

The shallower source, generating the highlighted pockmarks, is the impermeable clay layer constituting the Ribera Fm. The shallow fluids produced migrate to the seafloor with two different mechanisms: in the first one by dewatering and compaction of sediments, polygonal faults and focused emissions (e.g. gas chimneys) are generated; in the second they rise by diffusion through sandy lenses.

The distribution of the pockmark fields is not affected by structural control. Our morphometric analysis suggests instead a potential role of ABV current in shaping the elongated pockmarks field morphology.

Acknowledgements We are grateful to Copenhagen Offshore Partners (COP), 7 Seas Med srl, and FUGRO for making available the processed seismic dataset. Academic license of IHS Kingdom and MOVE 2021 have been used to research purposes. D.S. is founded by PON – 'Research and Innovation' 2014–2020. Thanks are due to the anonymous reviewers who helped improve the original manuscript.

Author contributions All authors wrote tha main manuscript text and reviewed the manuscript.

Data availability The High Penetration multi-channel seismic reflection dataset and well-log data are available at ViDEPI public database. The High Resolution seismic reflection profiles are available upon reasonable request at the University of Palermo (DiSTeM).

Declarations

Competing interests The authors declare no competing interests.

Conflict of interest The authors declare that they have no known conflict of interest.

References

Bachu S, Gunter WD, Perkins EH (1994) Aquifer disposal of CO2: hydrodynamic and mineral trapping. Energy Convers Manag 35(4):269–279

Béranger K, Mortier L, Gasparini GP, Gervasio L, Astraldi M, Crépon M (2004) The dynamics of the Sicily Strait: a comprehensive study from observations and models. Deep-Sea Res Part II: Topical Stud Oceanograp 51:411–440

Berndt C, Jacobs C, Evans A, Gay A, Elliott G, Long D, Hitchen K (2012) Kilometre-scale polygonal seabed depressions in the Hatton Basin, NE Atlantic Ocean: Constraints on the origin of polygonal faulting. Mar Geol 332:126–133

Bünz S, Polyanov S, Vadakkepuliyambatta S, Consolaro C, Mienert J (2012) Active gas venting through hydrate-bearing sediments on the Vestnesa Ridge, offshore W-Svalbard. Mar Geol 332–334:189–197

Cartwright J, Huuse M, Aplin A (2007) Seal bypass systems. AAPG Bull 91(8):1141–1166. https://doi.org/10.1306/04090705181

Cartwright JA (1994) Episodic basin-wide hydrofracturing of overpressured Early Cenozoic mudrock sequences in the North Sea Basin. Mar Pet Geol 11(5):587–607

Catalano R, Di Stefano P, Sulli A, Vitale FP (1996) Paleogeography and structure of the central Mediterranean: Sicily and its offshore area. Tectonophysics 260:291–323

Catalano R, Infuso S, Milia A, Sulli A (1993) The submerged Sicilian-Maghrebian chain along the Sardinia channel-Sicily straits belt. Geological development of the Sicilian-Tunisian Platform. UNESCO Rep Mar Sci 58:43–48

Cavallaro, D., Coltelli, M., 2019. The Graham volcanic field offshore southwestern Sicily (Italy) revealed by high-resolution seafloor mapping and ROV images. Frontiers in Earth Science.

Ceramicola S, Dupré S, Somoza L, Woodside J (2018) Cold Seep Systems. In: Micallef A, Krastel S, Savini A (eds) Submarine Geomorphology. Springer, Cham, pp 367–387

Civile D, Baradello L, Accaino F, Zecchin M, Lodolo E, Ferrante GM, Markezic N, Volpi V, Burca M (2023) Fluid-Related Features in the Offshore Sector of the Sciacca Geothermal Field (SW Sicily): The Role of the Lithospheric Sciacca Fault System. Geosciences 13(8):231

Civile D, Lodolo E, Accaino F, Geletti R, Schiattarella M, Giustiniani M, Fedorik J, Zecchin M, Zampa L (2018) Capo granitola-sciacca fault zone (Sicilian Channel, Central Mediterranean): structure vs magmatism. Mar Pet Geol 96:627–644

Civile D, Lodolo E, Alp H, Ben-Avraham Z, Cova A, Baradello L, Accettella D, Burca M, Centonze J (2014) Seismic stratigraphy and structural setting of the Adventure Plateau (Sicily Channel). Marine Geophysical Research 35:37–53

Civile D, Lodolo E, Caffau M, Baradello L, Ben-Avraham Z (2016) Anatomy of a submerged archipelago in the Sicilian Channel (central Mediterranean Sea). Geol Mag 153(1):160–178

Civile, D., Brancolini, G., Lodolo, E., Forlin, E., Accaino, F., Zecchin, M., Brancatelli, G. (2021). Morphostructural setting and tectonic evolution of the central part of the Sicilian Channel (central Mediterranean). Lithosphere. 2021 (1): 7866771. https://doi.org/10.2113/2021/7866771

Claypool, G.E., Kaplan, I.R., 1974. The Origin and Distribution of Methane in Marine Sediments, Natural Gases in Marine Sediments. Springer US, Boston, MA, pp. 99–139.

Coltelli, M., Cavallaro, D., D'Anna, G., D'Alessandro, A., Grassa, F., Mangano, G., Patanè, D., Gresta, S., 2016. Exploring the submarine graham bank in the sicily channel. Annals of Geophysics, 59.

Conte AM, Martorelli E, Calarco M, Sposato A, Perinelli C, Coltelli M, Chiocci FL (2014) The 1891 submarine eruption offshore Pantelleria Island (Sicily Channel, Italy): Identification of the vent and characterization of products and eruptive style. Geochem Geophys Geosyst 15(6):2555–2574

Corti G, Cuffaro M, Doglioni C, Innocenti F, Manetti P (2006) Coexisting geodynamic processes in the Sicily Channel. Special Papers-Geol Soc America 409:83

Davis AM (1992) Shallow gas: an overview. Cont Shelf Res 12:1077–1079

Etiope G, Milkov AV (2004) A new estimate of global methane flux from onshore and shallow submarine mud volcanoes to the atmosphere. Environ Geol 46:997–1002

Ferrante GM, Accaino F, Civile D, Lodolo E, Volpi V, Romeo R, Accettella D (2022) Deep and shallow gas occurrence in the NW Sicilian Channel and related features. Mar Pet Geol 139:105575

Fortibuoni, T., Bahri, T., Camilleri, M., Garofalo, G., Gristina, M., & Fiorentino, F., 2010 . Nursery and spawning Aïssi, M., Rovere, M., & Würtz, M., 2014. Sardinia channel—Strait of Sicily—Ionian Sea—Adriatic Sea seamounts. Atlas of Mediterranean Seamounts and Seamount-Like Structures.

Gafeira, J., Long, D., Diaz-Doce, D.J.N.S.G., 2012. Semi-automated characterisation of seabed pockmarks in the central North Sea. 10(4): 301–312.

Gardiner W, Grasso M, Sedgeley D (1995) Plio-pleistocene fault movement as evidence for mega-block kinematics within the Hyblean-Malta Plateau, Central Mediterranean. J Geodyn 19:35–51

Gasparini GP, Ortona A, Budillon G, Astraldi M, Sansone E (2005) The effect of the Eastern Mediterranean Transient on the hydrographic characteristics in the Strait of Sicily and in the Tyrrhenian Sea, Deep Sea Res. Part I 52:915–935. https://doi.org/10.1016/j.dsr.2005.01.001

Gasparo Morticelli M, Valenti V, Catalano R, Sulli A, Agate M, Avellone G, Albanese C, Basilone L, Gugliotta C (2015) Deep controls on foreland basin system evolution along the Sicilian fold and thrust belt. Bulletin De La Société Géologique De France 186:273–290

García Lafuente J, Garcìa A, Mazzola S, Quintanilla L, Delgado J, Cuttitta A, Patti B (2002) Hydrographic phenomena influencing early life stages of the Sicilian Channel Anchovy. Fish Oceanogr 11:31–44. https://doi.org/10.1046/j.1365-2419.2002.00186.x

Gauchery T, Rovere M, Pellegrini C, Cattaneo A, Campiani E, Trincardi F (2021) Factors controlling margin instability during the plio-quaternary in the Gela Basin (Strait of Sicily, Mediterranean Sea). Mar Pet Geol 123:104767

Gay A, Lopez M, Berndt C, Séranne M (2007) Geological controls on focused fluid flow associated with seafloor seeps in the Lower Congo Basin, Marine Geology, 244(1–4). ISSN 68–92:0025–3227. https://doi.org/10.1016/j.margeo.2007.06.003

Gentz T, Damm E, Schneider von Deimling J, Mau S, McGinnis DF, Schlüter M (2014) A water column study of methane around gas flares located at the West Spitsbergen continental margin. Cont Shelf Res 72:107–118

Grosse, P., van Wyk de Vries, B., Euillades, P.A., Kervyn, M., Petrinovic, I.A., 2012. Systematic morphometric characterization of volcanic edifices using digital elevation models. Geomorphology, 136, 114-131

Grosse, P., van Wyk de Vries, B., Petrinovic, I. A., Euillades, P. A., & Alvarado, G. E. (2009). Morphometry and evolution of arc volcanoes. Geology, 37(7), 651-654

Ho S, Cartwright JA, Imbert P (2012) Vertical evolution of fluid venting structures in relation to gas flux, in the Neogene-Quaternary of the Lower Congo Basin, Offshore Angola. Mar Geol 332–334:40–55

Hovland M, Heggland R, De Vries MH, Tjelta TI (2010) Unit-pockmarks and their potential significance for predicting fluid flow, Marine and Petroleum Geology, 27(6). ISSN 1190–1199:0264–8172. https://doi.org/10.1016/j.marpetgeo.2010.02.005

Hovland, M., 2011. The Geomorphology and nature of seabed seepage processes. Bathymetry and Its Applications, 79.

Hovland M, Gardner JV, Judd AG (2002) The significance of pockmarks to understanding fluid flow processes and geohazards. Geofluids 2:127–136

Hustoft S, Bünz S, Mienert J (2010) Three-dimensional seismic analysis of the morphology and spatial distribution of chimneys beneath the Nyegga pockmark field, offshore mid-Norway. Basin Res 22(4):465–480

Incarbona A., Di Stefano E., Patti B. , Pelosi N., Bonomo S., Mazzola S., Sprovieri R., Tranchida G., Zgozi S., Bonanno A., 2008. Holocene millennial-scale productivity variations in the Sicily Channel (Mediterranean Sea). Paleoceanography. . https://doi.org/10.1029/2007PA001581.

Istituto idrografico della Marina. Gênes, I., 1982. Atlante delle correnti superficiali dei mari italiani.

Judd A, Hovland M (1992) The evidence of shallow gas in marine sediments. Cont Shelf Res 12:1081–1095. https://doi.org/10.1016/0278-4343(92)90070-Z

Judd A, Hovland M (2007) Seabed Fluid Flow : The Impact on Geology. Cambridge University Press, Cambridge, Biology and the Marine Environment

Lermusiaux PFJ, Robinson AR (2001) Features of dominant mesoscale variability, circulation patterns and dynamics in the Strait of Sicily, Deep Sea Res. Part I 48:1953–1997. https://doi.org/10.1016/S0967-0637(00)00114-X

Loreto MF, Palmiotto C, Muccini F, Ferrante V, Zitellini N (2021) Inverted Basins by Africa-Eurasia Convergence at the Southern Back-Arc Tyrrhenian Basin. Geosciences 11(3):117

Løseth H, Gading M, Wensaas L (2009) Hydrocarbon leakage interpreted on seismic data, Marine and Petroleum Geology, 26(7). ISSN 1304–1319:0264–8172. https://doi.org/10.1016/j.marpetgeo.2008.09.008

Maiorana M, Artoni A, Le Breton E, Sulli A, Chizzini N, Torelli L (2023) Is the Sicily Channel a simple Rifting Zone? New evidence from seismic analysis with geodynamic implications. Tectonophysics 864:230019

Mattos NH, Alves TM, Omosanya KO (2016) Crestal fault geometries reveal late halokinesis and collapse of the Samson Dome, Northern Norway: Implications for petroleum systems in the Barents Sea. Tectonophysics 690:76–96

Micallef A, Averes T, Hoffmann J, Crutchley G, Mountjoy JJ, Person M, Cohen D, Woelz S, Bury SJ, Ahaneku CV, Spatola D, Luebben N, Miserocchi S, Krastel S, Torelli M, Omosanya KO (2022) Multiple drivers and controls of pockmark formation across the Canterbury Margin, New Zealand. Basin Res 34:1374–1399

Micallef A, Berndt C, Debono G (2011) Fluid flow systems of the Malta Plateau, Central Mediterranean Sea. Mar Geol 284:74–85

Micallef A, Spatola D, Caracausi A, Italiano F, Barreca G, D'Amico S, Petronio L, Coren F, Facchin L, Blanos R, Pavan A, Paganini P, Taviani M (2019) Active degassing across the Maltese Islands (Mediterranean Sea) and implications for its neotectonics. Mar Petrol Geol. https://doi.org/10.1016/j.marpetgeo.2019.03.033

Milia A, Iannace P, Torrente MM (2021) The meeting place of backarc and foreland rifting: the example of the offshore western Sicily (Central Mediterranean). Global Planet Change 198:103408

Miramontes E, Cattaneo A, Jouet G, Théreau E, Thomas Y, Rovere M, Cauquil E, Trincardi F (2016) The Pianosa Contourite Depositional System (Northern Tyrrhenian Sea): Drift morphology and Plio-Quaternary stratigraphic evolution. Mar Geol 378:20–42

Motyka RJ, Poreda RJ, Jeffrey A (1989) Geochemistry, isotopic composition, and origin of fluids emanating from mud volcanoes in the Copper River basin. Alaska 53(1):29–41

Parrino N, Burrato P, Sulli A, Gasparo Morticelli M, Agate M, Srivastava E, Malik JN, Di Maggio C (2023) Plio-Quaternary coastal landscape evolution of north-western Sicily (Italy). J Maps 19:1. https://doi.org/10.1080/17445647.2022.2159889

Pennino V, Sulli A, Caracausi A, Grassa F, Interbartolo F (2014) Fluid escape structures in the north Sicily continental margin. Mar Pet Geol 55:202–213

Picard K, Radke LC, Williams DK, Nicholas WA, Siwabessy PJ, Howard FJF, Gafeira J, Przeslawski R, Huang Z, Nichol S (2018) Origin of high density seabed pockmark fields and their use in inferring bottom currents. Geosciences 8:195

Robinson, A.R., Leslie, W.G., Theocharis, A., Lascaratos, A., 2001. Mediterranean Sea Circulation. Encyclopedia of Ocean Sciences, 1–19.

Ruiz CR, García-Cacho L, Araña V, Luque AY, Felpeto A (2000) Submarine volcanism surrounding Tenerife, Canary Islands: Implications for tectonic controls, and oceanic shield formingprocesses. J Volcanol Geoth Res 103:105–119

Santinelli, C. (2015). DOC in the Mediterranean Sea. In Biogeochemistry of marine dissolved organic matter (pp. 579–608). Academic Press.

Savini A, Malinverno E, Etiope G, Tessarolo C, Corselli C (2009) Shallow seep-related seafloor features along the Malta plateau (Sicily channel - Mediterranean Sea): Morphologies and geo-environmental control of their distribution. Mar Pet Geol 26:1831–1848

Spatola, D., Micallef, A., Sulli, A., Basilone, L., Basilone, G., 2017. Gathering different marine geology data (seismics, acoustics, sedimentological) to investigate active fluid seepage (AFS) in the southern region of the central Mediterranean Sea, IMEKO TC19 Workshop on Metrology for the Sea, MetroSea 2017: Learning to Measure Sea Health Parameters.

Spatola D, Micallef A, Sulli A, Basilone L, Basilone G (2018a) Evidence of active fluid seepage (AFS) in the southern region of the central Mediterranean Sea. Measurement 128:247–253

Spatola D, Micallef A, Sulli A, Basilone L, Ferreri R, Basilone G, Bonanno A, Pulizzi M, Mangano S (2018b) The Graham Bank (Sicily Channel, central Mediterranean Sea): Seafloor signatures of volcanic and tectonic controls. Geomorphology 318:375–389

Spatola D, Sulli A, Basilone L, Casalbore D, Napoli S, Basilone G, Chiocci FL (2023) Morphology of the submerged Ferdinandea Island, the 'Neverland'of the Sicily Channel (central Mediterranean Sea). J Maps 19(1):2243305

Sulli A, Morticelli MG, Agate M, Zizzo E (2021) Active north-vergent thrusting in the northern Sicily continental margin in the frame of the quaternary evolution of the Sicilian collisional system. Tectonophysics 802:228717

Sulli A, Zizzo E, Spatola D, Morticelli MG, Agate M, Iacono CL, Gargano F, Pepe F, Ciaccio G (2020) Growth and geomorphic evolution of the Ustica volcanic complex at the Africa-Europe plate margin (Tyrrhenian Sea). Geomorphology 374:107526

Sun Q, Wu S, Hovland M, Luo P, Lu Y, Qu TJM, Geology P (2011) The morphologies and genesis of mega-pockmarks near the Xisha Uplift. South China Sea 28(6):1146–1156

Sun X, Yang J, Zheng M, Zhang X (2020) Artificial construction of the biocoenosis of deep-sea ecosystem via seeping methane. Environ Microbiol 00:1–13

Tinivella U, Loreto MF, Accaino F (2009) Regional versus detailed velocity analysis to quantify hydrate and free gas in marine sediments. South Shetland Margin Case Study. https://doi.org/10.1144/SP319.9

Todaro, S., Sulli, A., Spatola, D., Basilone, G., Aronica, S., 2022. Seismic stratigraphy of the north-westernmost area of the Malta Plateau (Sicily Channel): The Middle Pleistocene-Holocene sedimentation in a tidally influenced shelf. Marine Geology, 106740.

Todaro S, Sulli A, Spatola D, Micallef A, Di Stefano P, Basilone G (2021) Depositional mechanism of the upper Pliocene-Pleistocene shelf-slope system of the western Malta Plateau (Sicily Channel). Sed Geol 417:105882

VIDEPI Project, V., 2012. Visibility of petroleum exploration data in Italy. Ministry for Economic Development DGRME—Italian Geological Society—Assomineraria.

Volpi V, Civile D, Lodolo E, Romeo R, Accettella D, Accaino F, Ferrante GM (2022) Seabed and shallow morphological setting of the western Sicilian Channel. Bullet Geophys Oceanograp 63(3):357–376

Whiticar MJ (1999) Carbon and hydrogen isotope systematics of bacterial formation and oxidation of methane. Chem Geol 161:291–314

Whiticar MJ (2002) Diagenetic relationships of methanogenesis, nutrients, acoustic turbidity, pockmarks and freshwater seepages in Eckernförde Bay. Mar Geol 182:29–53

Zitellini N, Ranero CR, Loreto MF, Ligi M, Pastore M, D'Oriano F, Sallares V, Grevemeyer I, Moeller S, Prada M (2020) Recent inversion of the Tyrrhenian Basin. Geology 48(2):123–127